Polarized radio emission over the southern Galactic plane at 2.4 GHz

A. R. Duncan,[1] R. F. Haynes,[2] K. L. Jones[1] and R. T. Stewart[2]

[1]*Physics Department, The University of Queensland, QLD 4072, Australia*
[2]*Australia Telescope National Facility, CSIRO, PO Box 76, Epping, NSW 2121, Australia*

ABSTRACT
Polarimetric results from the Parkes 2.4-GHz survey of the southern Galactic plane are presented. These take the form of a series of images, detailing the polarized intensity and vector position angles over the survey area. The observations were made using the 64-m Parkes radio telescope, and cover the Galactic plane within the region $238° \leq l \leq 5°$, with a latitude range of at least $|b| \leq 5°$, with some coverage to $b = +7°$ and $b = -8°$. The resolution of the images is 10.4 arcmin. The rms noise of the polarized intensity images is 11 mJy beam area^{-1} (5.3 mK), and the rms variation in the vector position angles is of the order of several dgrees. The images show many polarized structures, over a wide range of intensities and angular sizes. Bright, extended regions of polarized emission (of the order of 5° across) are detected, including the Vela supernova remnant and a large 'cap' structure appearing to the north of Sgr A. A quasi-uniform 'background' component of faint, patchy emission is seen over the length of the survey. This faint component appears to originate over a range of distances, out to greater than 5 kpc, and shows considerable structure in the orientations of the polarization vectors. Several bright H II complexes are seen to exhibit bipolar, depolarizing 'plumes', several degrees in length, which are interpreted as outflows of low-density thermal material (with densities in the range 1–10 cm^{-3}).

Key words: polarization – surveys – supernova remnants – Galaxy: structure.

1 INTRODUCTION

Polarimetric surveys provide a lot of information about the radiation they detect and, from this, certain characteristics of both the interstellar medium (ISM) and the emission regions themselves can be deduced. Specifically, polarimetric data can provide information on the field uniformity and non-thermal electron distribution within the emission regions, and the angular scales of variation in these quantities. Coupled with other information, polarimetric observations can also assist in determining the orientations of the tangential magnetic field component within the emitting regions, as well as magnetic field strengths and the densities of both thermal and non-thermal electrons.

In this paper, the polarimetric results from the recent Parkes 2.4-GHz survey of the southern Galactic plane are presented. The total-power data, along with a detailed description of the survey, were given by Duncan et al. (1995; hereafter referred to as Paper I). The basic results presented here are a series of images detailing both the intensity of the polarized emission and the orientation of the polarization vectors along the southern plane. The characteristics and features of the images are then identified, and the possible origins of the polarized emission discussed.

2 THE PARKES SURVEY

The Parkes 2.4-GHz survey is a sensitive, polarimetric survey of the southern Galactic plane, observed with the 64-m Parkes telescope. The survey details 127° of Galactic longitude ($238° \leq l \leq 5°$), with a latitude coverage out to at least $\pm 5°$ (over some longitudes, this is extended to $b = +7°$ or $b = -8°$). The angular resolution of the images is 10.4 arcmin. Some parameters of the survey are listed in Table 1.

The polarized intensity images presented herein have a nominal rms noise (see Table 1) of 11 mJy beam area^{-1} (5.3 mK). The errors in the polarization vector orientations depend to a large degree on the polarized intensity at each point, but are generally of the order of a few degrees (see Table 1). For a 2σ detection of polarized emission (22 mJy beam area^{-1}), below which vectors are not plotted, the uncertainty in the position angle is approximately $\pm 10°$.

Table 1. Information pertaining to the polarimetric survey. Note that the rms noises are quoted for beam areas calculated from the final map beamwidth. P is the polarized intensity, in mJy beam area^{-1}. Areas of nominal rms noise are shown with a herringbone pattern in Fig. 1, while those of lower rms noise (primarily blocks 1 and 4) are shown as black in Fig. 1. The major axis of the beam is oriented parallel to the Galactic plane.

System temperature	$\simeq 40$ K
Centre frequency	2.417 GHz
Bandwidth	145 MHz
Telescope beamwidth	$(8.93 \times 8.40) \pm 0.08$ (HPBW)
Final map beamwidth	$(10.62 \times 10.23) \pm 0.07$ (HPBW)
Nominal rms noise	11 mJy beam area^{-1}
brightness temperature	5.3 mK
Blocks 1 and 4 rms noise	6 mJy beam area^{-1}
brightness temperature	2.9 mK
Nominal pos'n angle error	$\left(4 + \dfrac{5 \times 10^4}{P^2}\right)^{0.5}$ degrees
Blocks 1 and 4 angle error	$\left(4 + \dfrac{1.5 \times 10^4}{P^2}\right)^{0.5}$ degrees

This uncertainty falls rapidly, reaching $\pm 5°$ for a 5σ (55 mJy beam area^{-1}) detection. At polarized intensities of the order of 100 mJy beam area^{-1} and greater, the error is dominated by the $\pm 2°$ uncertainty in the absolute calibration of the position angles.

2.1 Previous investigations

Since the early 1960s, a large number of surveys of the linearly polarized emission from the Galaxy have been made (e.g. Westerhout et al. 1962; Wielebinski & Shakeshaft 1964; Berkhuijsen et al. 1965; Spoelstra 1971; Brouw & Spoelstra 1976). The aim of most of these surveys was to investigate the large-scale polarization characteristics of the Galaxy, and hence large areas of sky were usually observed with resolutions of only a few degrees. Almost all of these early polarimetric surveys covered the northern sky only; the only large-area survey of polarization in the south is the 408-MHz work of Mathewson & Milne (1965).

High-resolution surveys into the polarimetric characteristics of the Galactic plane are comparatively rare. The largest investigation to date is the work of Junkes, Fürst & Reich (1987a), which presents polarimetric results over a section of the plane defined by $4°9 \leq l \leq 76°$, with $|b| \leq 1°5$, at a frequency of 2.695 GHz. The only other similar investigations were a series of surveys surrounding the Galactic Centre at 3-cm wavelengths, covering approximately $3° \times 3°$, by Tsuboi et al. (1986) and Haynes et al. (1992).

The 327-MHz observations of Wieringa et al. (1993) provide the highest resolution insights into the small-scale structure of the Galactic polarized emission. However, only a few areas of sky were examined in this work, none larger than a degree or so across.

It should be noted that no previous survey has examined the polarimetric characteristics of the southern Galactic plane at these resolutions, and also that no previous work

has investigated these characteristics over a latitude range of $|b| \leq 5°$, for any section of the plane.

3   RECEIVER AND POLARIMETER

Observations were made using a two-channel, cooled, high electron mobility transistor (HEMT) receiver system. Based on the prototype for the Australia Telescope Compact Array, this wide-bandwidth receiver exhibits superb phase and gain stability, with a system temperature of approximately 40 K (Sinclair et al. 1992).

A detailed description of the receiver and polarimeter is given in Paper I. Briefly, signals are fed into the receiver from a pair of orthogonal, linear probes situated in the waveguide behind the feed. These probes are preceded by a quarter-wave plate. The received signals pass through the dewar and low-noise amplifiers, and are then split by power dividers before entering the total-power and polarization stages of the polarimeter. Stokes parameters Q and U are generated by quadrature phase switching and correlation of the two input signals.

Also present in the waveguide is a linear calibration probe, oriented at $45°$ to both receiver probes, which injects noise equally into each of the two channels. The injection of this calibration signal (every alternate 130 ms) allows quasi-continuous calibration of the receiving system.

A phase switch periodically reverses the sign of all correlations within the polarization stage (every 65 ms), which assists in eliminating any residual offset terms.

4   OBSERVATIONS

All observations were undertaken using the 64-m Parkes radio telescope, operating at a centre frequency of 2.417 GHz and a receiver bandwidth of 145 MHz. The total extent of the surveyed area is shown graphically in Fig. 1. Four separate observing sessions were required to complete the survey (see Paper I for details).

Observations were made by scanning the telescope in the directions of constant Galactic latitude (b) and constant Galactic longitude (l), at a rate of $6°$ per minute. A separation between adjacent scans of 4 arcmin was used throughout the survey, as this provided more than 2.1 points per beamwidth (above the Nyquist rate).

The large range of Galactic longitude covered by the observations necessitated dividing the survey strip into six 'blocks', each of which covers approximately $20°$ of Galactic longitude (see Paper I for more information). Each point in the survey was observed at least twice: once using constant-longitude scans (l-scans) and once with constant-latitude scans (b-scans). These orthogonally scanned maps (l-maps and b-maps) were later compared and combined in order to suppress low-level scanning effects and noise.

Throughout the observations, two sources were regularly observed as gain calibrators: $1934 - 638$ and Hydra A. These were assumed (Kühr et al. 1981) to have flux densities of 11.50 and 25.87 Jy at the observing frequency, respectively, agreeing well with the Baars et al. (1977) flux density scale. Note that the value for $1934 - 638$ takes into account the changes recommended by Reynolds (1994). This absolute scaling is accurate to within approximately 1 per cent (Reynolds 1994).

The polarization calibrator chosen for the survey was the source 3C 138, which has a fractional polarization of approximately 8 per cent and a position angle of 169° (Tabara & Inoue 1980) at 2.4 GHz.

Additionally, observations were made of the point-like H II region 0605 − 063, to determine the level of instrumental polarization. Since this source is an H II region, we expect its emission to be completely unpolarized, and hence any polarization observed in 0605 − 063 must be an artefact of the observing system. Based on observations of this source, the instrumental polarization was estimated to be ≈ 0.5 per cent.

During the observations of 1994 March, we experienced almost continuous, low-level interference, which resulted in the rms noise of the unprocessed maps rising to a value of approximately twice that of our other observing sessions. Consequently, some areas of the survey have a higher rms noise than other regions; these are detailed in Fig. 1.

5 DATA REDUCTION

The NOD2 reduction system (Haslam 1974) was used throughout for processing the observations and producing the final images.

Much of the initial data reduction for the Stokes Q and U images is identical to that of the total-power data, which is described in Paper I and need not be repeated here. Specifically, assembling the individual scans into maps, scaling these maps against the amplitude calibrators, and careful baselining of both the l-maps and b-maps are all essentially the same as the total-power reduction procedures.

Each map was carefully examined for discontinuities, noise spikes, interference or other problems. Orthogonally scanned maps were often compared to distinguish bad data from real structures. If affected pixels were found in areas of the maps containing simple structure, these were corrected by interpolation with adjacent values. Otherwise, the pixels were flagged out.

At this point, the reduction procedure for the Stokes Q and U data diverged from that of the total-power data. In each block, l- and b-scanned maps of both Q and U components existed. Before combining these to form the polarization images, the instrumental polarization effects were removed.

5.1 Instrumental polarization

When the telescope scans across an unpolarized source, of the order of 0.5 per cent of the received total-power flux is detected in polarized intensity. Indeed, the greatest defects

in the Stokes Q and U images are caused by this instrumental polarization surrounding bright, discrete sources – with point-like sources exhibiting the distinctive 'butterfly' pattern, an example of which is shown in Fig. 2. Only sources with total-power flux densities exceeding 3 Jy beam area^{-1} were found to have a detectable level of instrumental polarization.

To remove the instrumental effects, an estimate of the instrumental component of the polarization must first be made. This was done by convolving the total-power image with the Q and U responses of the telescope to a bright, unpolarized, point-like source; the convolution kernels actually used are shown in Fig. 2. For each block of the survey, this process produced maps detailing both the Q and U responses of the telescope to the total-power emission seen within the field.

The areas surrounding bright sources that could be seen to be affected by instrumental polarization were then selected, and a NOD2 program specifically designed for the task was used to remove the instrumental effects. The program examined the maps of the instrumental component within each selected region, and determined the optimum scaling factors and rotation angles for the 'butterfly' patterns, to minimize (in the least-squares sense) the residual polarized flux from each area.

This process worked reasonably well around most sources; however, very bright emission regions (such as near Sgr A and the bright H II complexes between longitudes 280° and 295°) can leave large residuals in the cleaned images. These residuals result from both errors in telescope positioning (± 15 arcsec rms) and errors in the measured Stokes Q and U point-source responses (shown in Fig. 2). Around bright regions such as these, the data have been blanked.

It is also of interest to examine the instrumental polarization associated with the large-scale background emission component, which appears in fig. 4 of Paper I. Near the Galactic Centre, the maximum amplitude of this large-scale component is approximately 7.5 Jy beam area^{-1} (taking a relative zero for the large-scale emission at $b = \pm 5°$). In order to determine the instrumental polarization arising from this component, the large-scale emission was convolved with the Stokes Q and U point-source responses of the telescope. It was found that the level of instrumental polarization for this large-scale emission was less than that of the smaller scale emission and sources – by a factor of approximately 3 to 4. That is, where a point-like or extended source produced a polarized response at about the 1 per cent level, the large-scale background emission component produced an instrumental polarization at approximately the 0.3 per cent level.
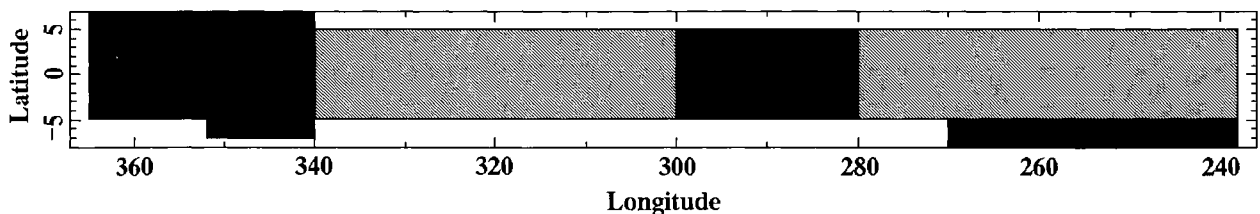
Figure 1. Darkened areas show regions of the Galactic plane covered by the survey. Grey areas indicate the nominal rms noise of 11 mJy beam area^{-1}, while black denotes the lower rms noise of 6 mJy beam area^{-1}. Axis markings are in degrees.
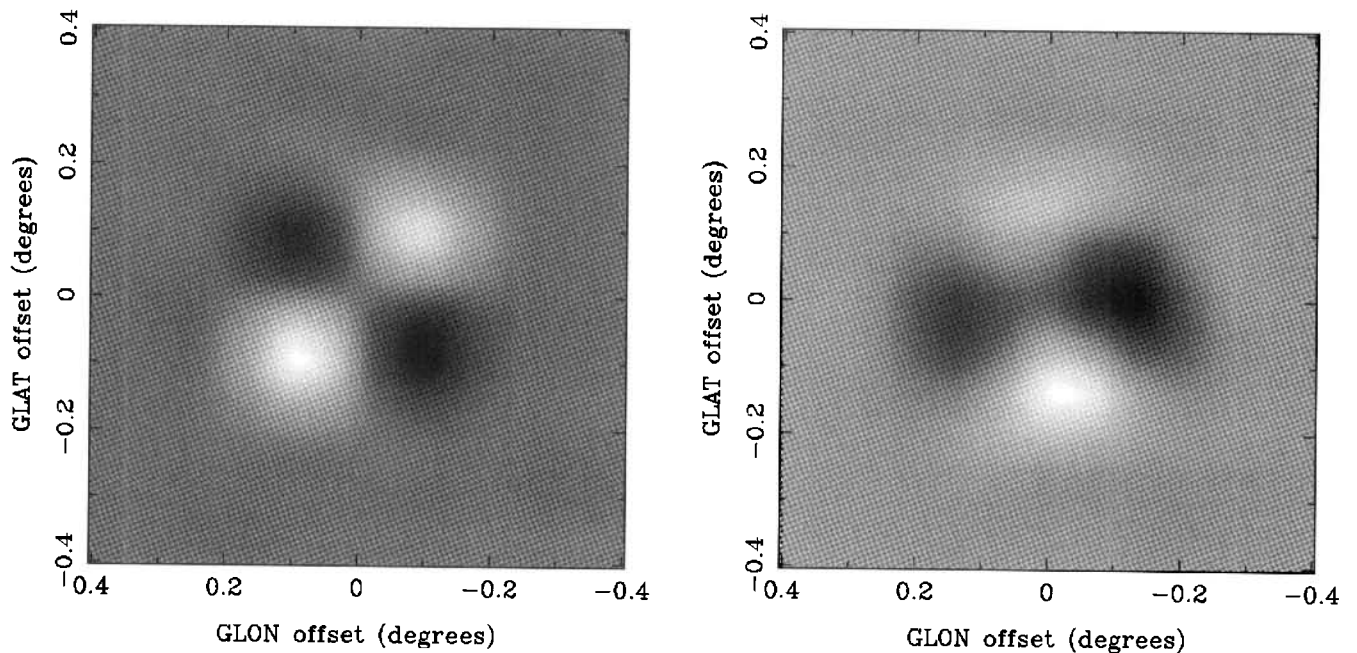
Figure 2. Left panel: the Stokes Q; right panel: Stokes U beams of the Parkes radio telescope, as determined from the 2.4-GHz survey. Note the distinctive 'butterfly' shape.

Near Sgr A, then, where this large-scale emission is brightest, an instrumental polarized flux of about 23 mJy beam area^{-1} (approximately 2σ) is expected. More than 2° away from the Galactic Centre the intensity of this broad-scale emission falls rapidly, reducing any instrumental polarization to correspondingly smaller levels. Confirmation that the instrumental component of the background emission is a small effect can be found in the polarized intensity images presented in the following section. Nowhere along the survey can a significant 'ridge' of polarized emission be seen near $b = 0°$, even near the Galactic Centre where the background component is strongest. Hence no attempt was made to remove instrumental polarization from the large-scale, background emission.

5.2 Forming the images

After removing the instrumental polarization, each pair of l- and b-scanned maps was then combined using the PLAIT software of Emerson & Gräve (1988). Note that, if two blanked regions are combined, the result will also be blanked; however, if a blanked region is combined with an area containing valid pixels, the valid data will appear in the output map.

The overlap regions of adjacent blocks were examined and it was confirmed that no discontinuities existed at block boundaries; hence no extra base levels were added. All the blocks were then combined to form the survey 'strip', 127° in length. To improve the signal-to-noise ratio, both the Stokes Q and U surveys were then smoothed with a Gaussian which increased the effective beamwidth to 1.2 times the telescope beamwidth (see Table 1), and appropriately rescaled.

The polarized intensity and position angle images (Figs 3–8) were then calculated from the corresponding Q and U images.

It should be noted that the reduction techniques used here attenuate structure on angular scales of the order of 20° and larger. In the case of the total-power images, this could be recovered by comparison with the 2.3-GHz survey of Jonas, de Jager & Baart (1985). Unfortunately, no similar survey of comparable sensitivity exists for Stokes Q or U data, and hence no attempt has been made to restore any of this low-spatial-frequency polarized emission. Therefore it must be stressed that any polarized components with angular scales of the order of 20° and greater will not be correctly represented in the survey data.

6   RESULTS AND DISCUSSION

The polarimetric images of each block are shown in Figs 3 to 8. These figures detail both the polarized intensities and the orientations of the polarization vectors (magnetic vectors) of the emission. In the absence of significant Faraday rotation, the orientation of these **B** vectors will be parallel with the direction of the magnetic field within the emitting region (averaged over the telescope beam). No filtering or background subtraction has been applied to any of the data presented here.

The nominal brightness sensitivity of the polarized intensity images is approximately 10^{-23} W m^{-2} Hz^{-1} sr^{-1} (1000 Jy sr^{-1}). This is a sensitivity increase over the 11-cm Effelsberg survey work (Reich et al. 1984; Junkes et al. 1987a) of approximately a factor of 5.

6.1   Overview of the images

The images reveal a myriad of polarized structures, over a wide range of intensities and angular sizes. Some of the most intense emission is seen around 265° longitude, and is associated with the Vela supernova remnant (SNR): see
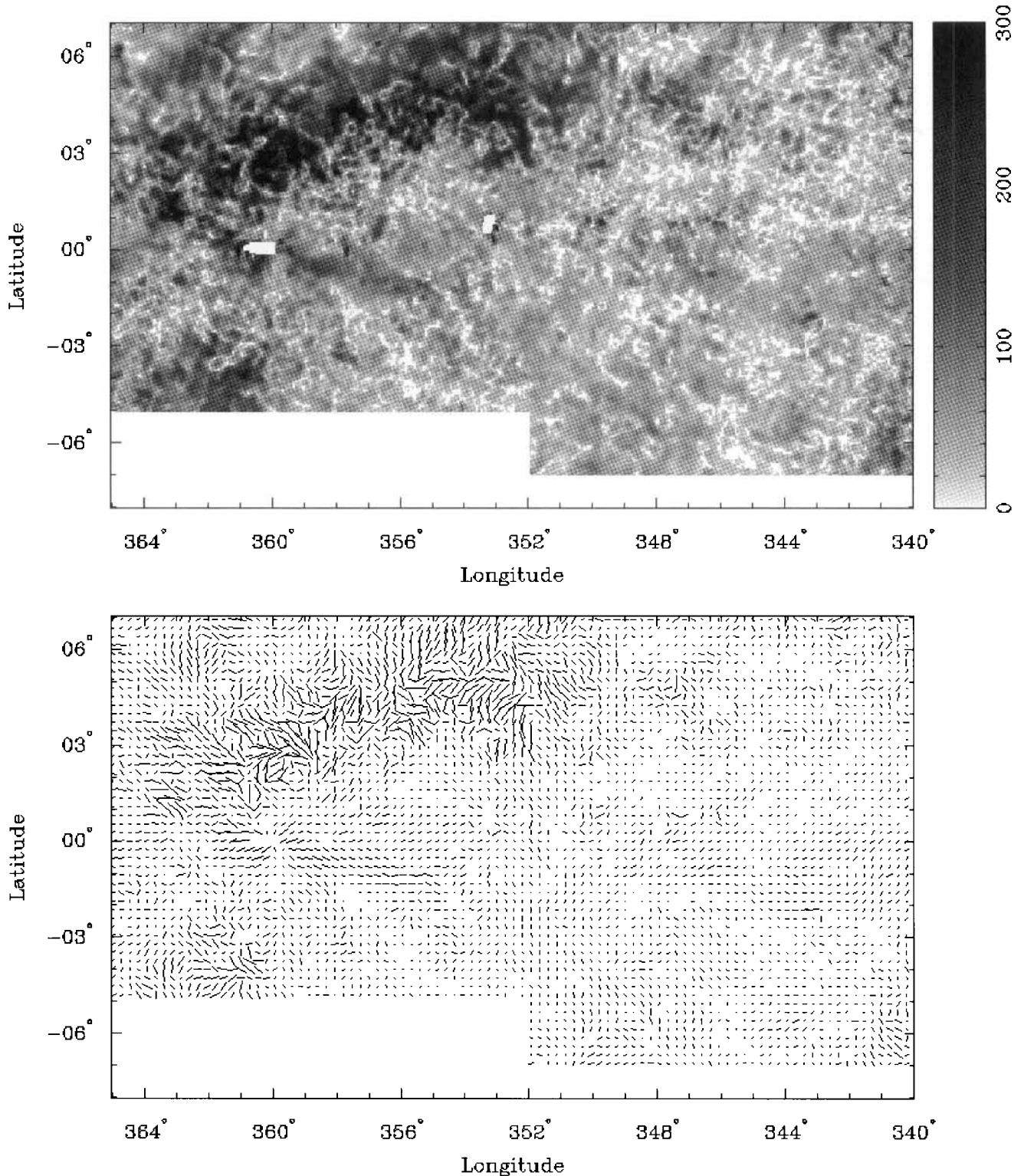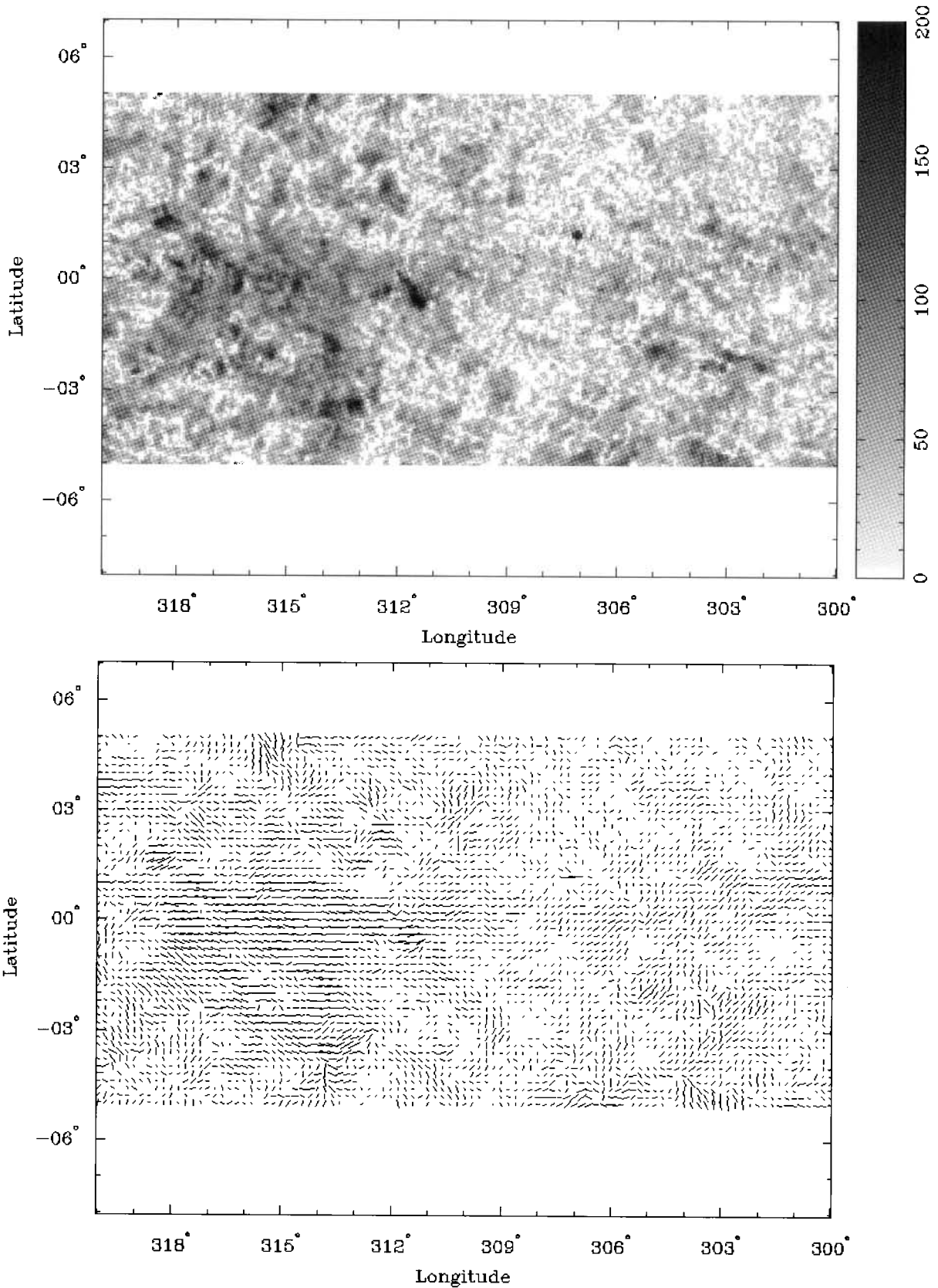
Figure 3. Top panel: grey-scale image detailing the polarized intensities detected over the region of the plane $5° \geq l \geq 340°$. The grey-scale wedge is labelled in mJy beam area^{-1}. The image is blanked in the vicinity of Sgr A and the bright H ɪɪ complex near G353.2 + 0.8; note that some instrumental polarization may be present close to the blanked regions. Bottom panel: polarization position angles over the same region. The orientation of the magnetic vector of the received radiation is shown. The length of each vector is proportional to the intensity of the polarized emission at each point, with a maximum polarized intensity of 430 mJy beam area^{-1}. Data are blanked wherever the polarized intensity falls below 2σ. A vector is plotted for every fourth pixel.
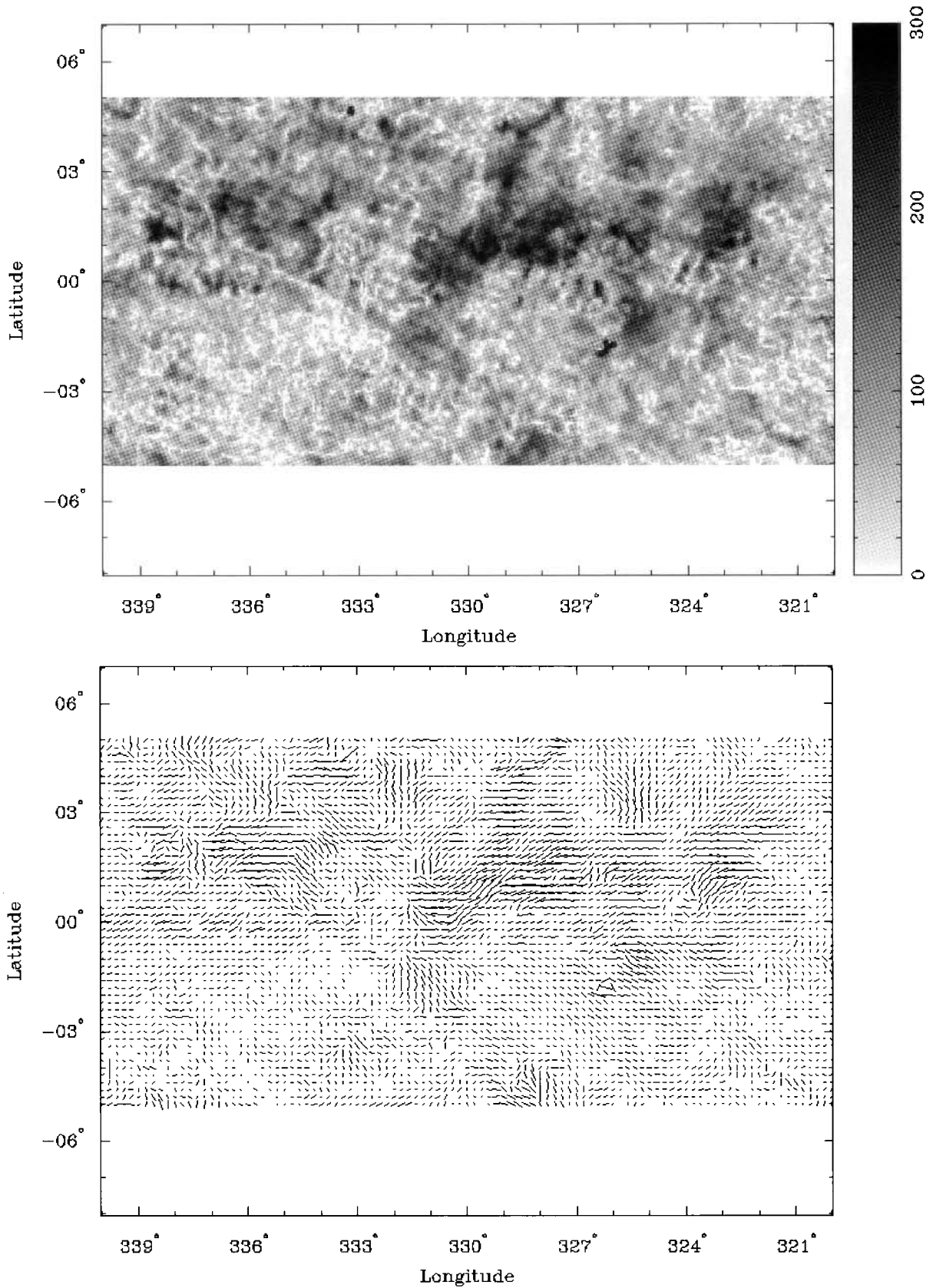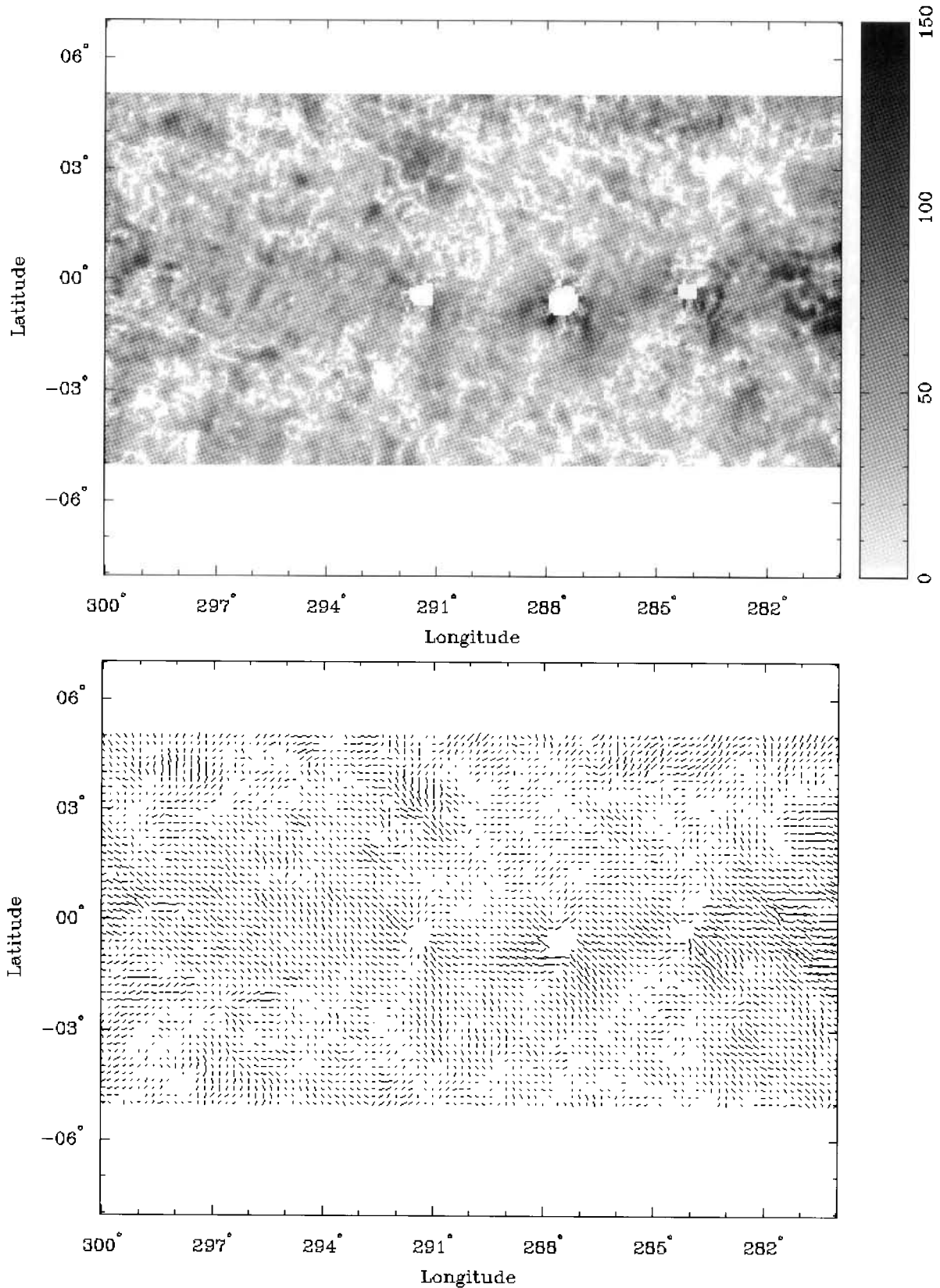
Figure 4. Top panel: grey-scale image detailing the polarized intensities detected over the region of the plane $340° \geq l \geq 320°$. The grey-scale wedge is labelled in mJy beam area^{-1}. Bottom panel: polarization position angles over the same region. The orientation of the magnetic vector of the received radiation is shown. The length of each vector is proportional to the intensity of the polarized emission at each point, with a maximum polarized intensity of 465 mJy beam area^{-1}. Data are blanked wherever the polarized intensity falls below 2σ. A vector is plotted for every third pixel.
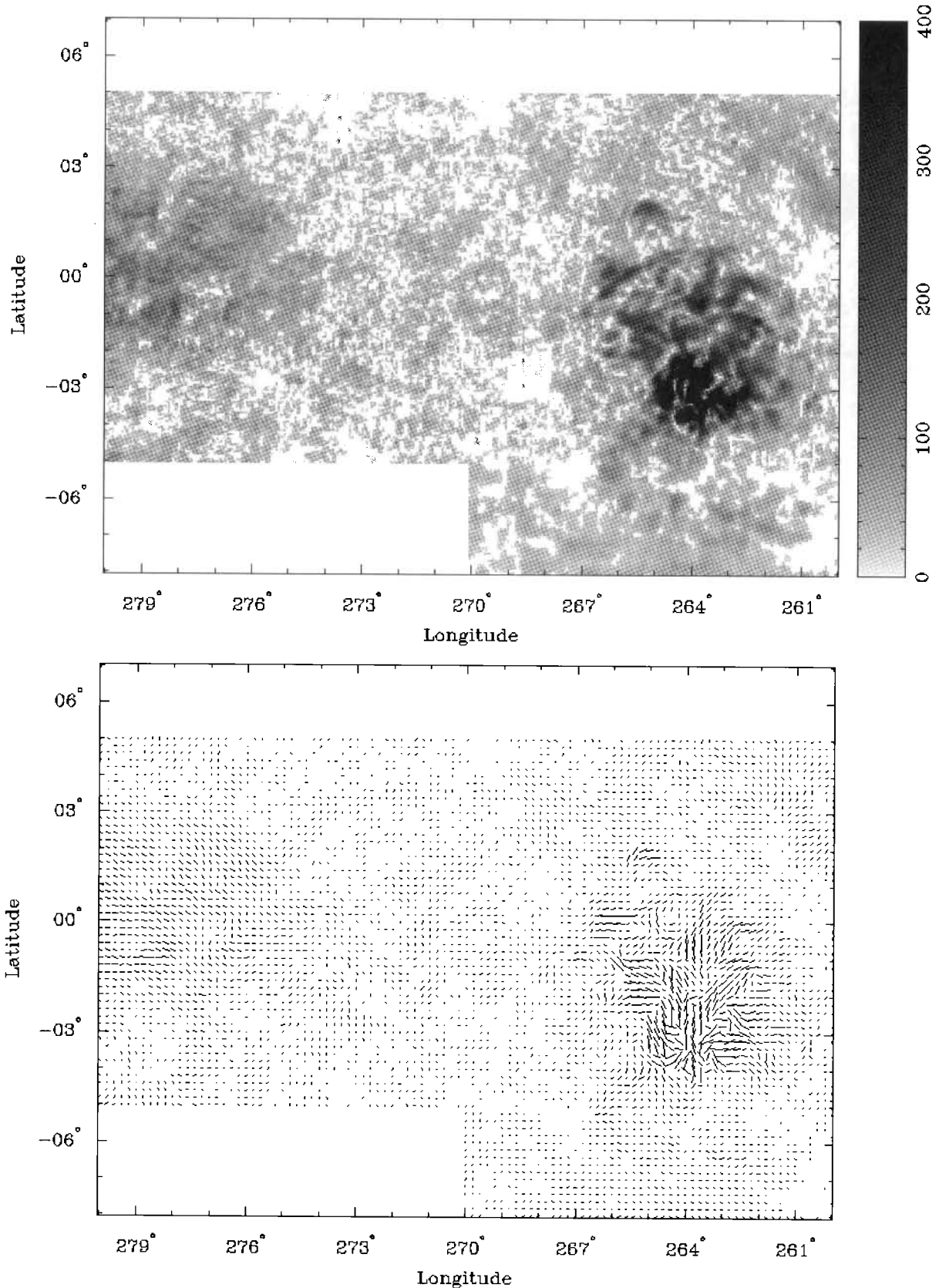
Figure 5. Top panel: grey-scale image detailing the polarized intensities detected over the region of the plane $320° \geq l \geq 300°$. The grey-scale wedge is labelled in mJy beam area^{-1}. Bottom panel: polarization position angles over the same region. The orientation of the magnetic vector of the received radiation is shown. The length of each vector is proportional to the intensity of the polarized emission at each point, with a maximum polarized intensity of 365 mJy beam area^{-1}. Data are blanked wherever the polarized intensity falls below 2σ. A vector is plotted for every third pixel.
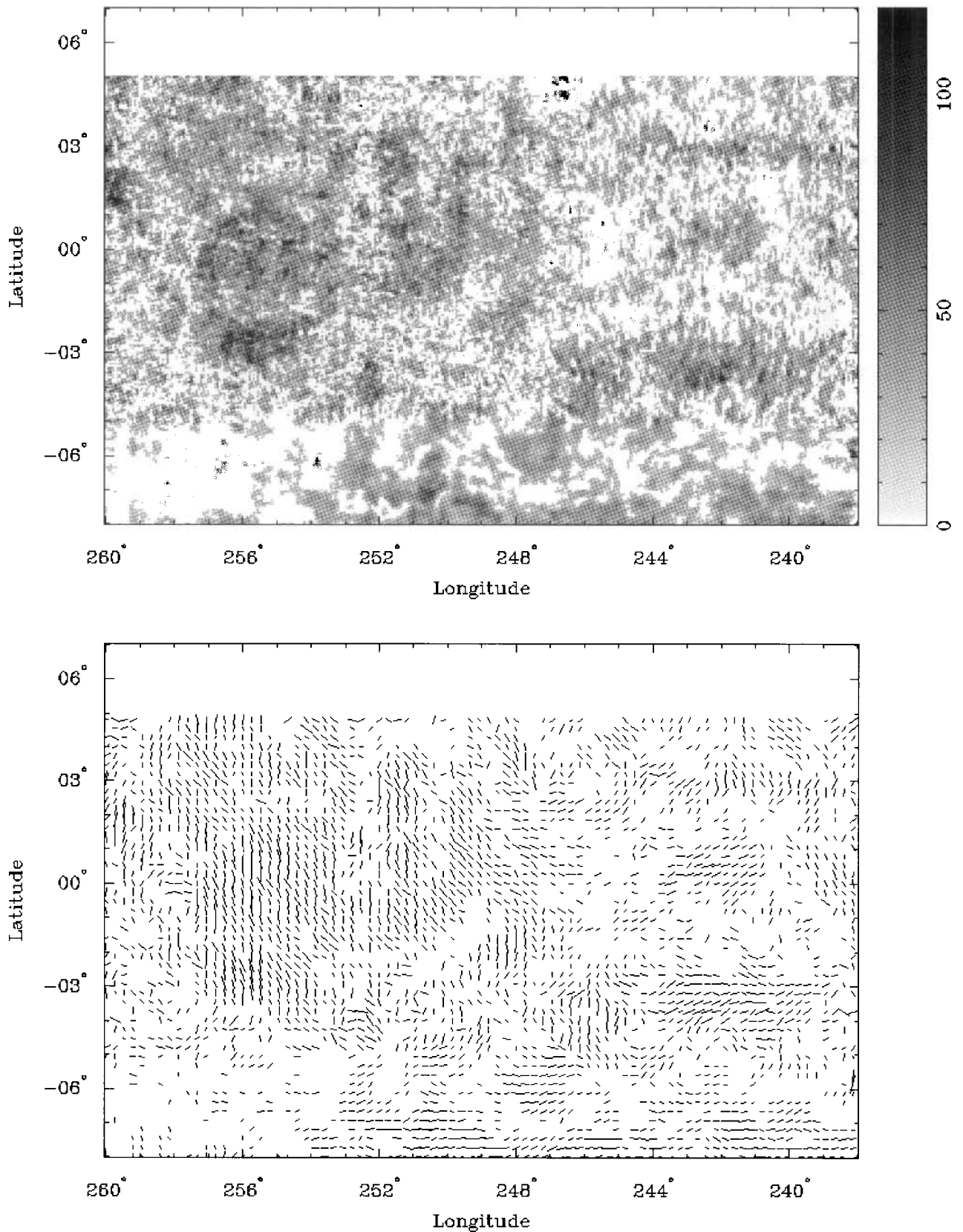
Figure 6. Top panel: grey-scale image detailing the polarized intensities detected over the region of the plane $300° \geq l \geq 280°$. The grey-scale wedge is labelled in mJy beam area^{-1}. The image is blanked in the vicinity of the three brightest H ɪɪ complexes; note that some instrumental polarization may be present in the vicinity of the blanked regions. Bottom panel: polarization position angles over the same region. The orientation of the magnetic vector of the received radiation is shown. The length of each vector is proportional to the intensity of the polarized emission at each point, with a maximum polarized intensity of 157 mJy beam area^{-1}. Data are blanked wherever the polarized intensity falls below 2σ. A vector is plotted for every third pixel.

Figure 7. Top panel: grey-scale image detailing the polarized intensities detected over the region of the plane $280° \geq l \geq 260°$. The grey-scale wedge is labelled in mJy beam area^{-1}. Bottom panel: polarization position angles over the same region. The orientation of the magnetic vector of the received radiation is shown. The length of each vector is proportional to the intensity of the polarized emission at each point, with the maximum polarized intensity clipped at 300 mJy beam area^{-1} to avoid overly long vectors. (The true maximum polarized intensity is 1.7 Jy beam area^{-1}.) Data are blanked wherever the polarized intensity falls below 2σ. A vector is plotted for every third pixel.

Figure 8. Top panel: grey-scale image detailing the polarized intensities detected over the region of the plane $260° \geq l \geq 238°$. The grey-scale wedge is labelled in mJy beam area^{-1}. Bottom panel: polarization position angles over the same region. The orientation of the magnetic vector of the received radiation is shown. The length of each vector is proportional to the intensity of the polarized emission at each point, with a maximum polarized intensity of 125 mJy beam area^{-1}. Data are blanked wherever the polarized intensity falls below 2σ. A vector is plotted for every fourth pixel.

Duncan et al. (1996). Polarized emission is also visible from other known SNRs, such as G326.3–1.8 (Clark, Green & Caswell 1975; Milne et al. 1989) and G343.1–2.3 (McAdam, Osborne & Parkinson 1993; Frail, Goss & Whiteoak 1994), and polarized extragalactic sources, such as G333.2 + 4.7. However, some of the most striking features of the images are the extended areas of polarization, with sizes of the order of 5° or so, which do not appear to be connected with discrete sources of total-power emission. Several examples of such regions are visible in the survey images, with the brightest lying near longitudes of 280°, 320° to 330°, and 355° to 5°.

Aside from the bright regions of extended polarization, the survey data reveal faint, diffuse polarized emission over much of the plane, often distributed in a patchy or clumpy manner. Over the western end of the survey, around longitudes of 240° to 260°, much of the faint polarization appears to be associated with the Gum nebula (Duncan et al. 1996). Nevertheless, similar faint and patchy emission is seen over large areas of the plane, out to essentially the latitude limit of the survey and presumably beyond.

At this point, it is convenient to break the polarized emission we see in the images into two categories: 'bright' and 'faint'. The brightest features are generally discrete structures, such as the Vela SNR or the brightly polarized region seen at high latitudes near $l = 0°$. By contrast, much of the faint emission is patchy and diffuse, and appears distributed quasi-uniformly over large areas of the survey.

These bright and faint features will be discussed later. First, however, it is of interest to examine quantitatively the distributions of both polarized intensity and vector orientation with Galactic longitude.

6.1.1 Distribution of polarized intensities

The distribution of polarized intensity values along the plane, averaged into 1° intervals of Galactic longitude, is shown in Fig. 9. Two lines are shown: the solid line depicts the mean polarized intensity values for $|b| \leq 2°$, and the dashed line shows the mean polarized intensities from the survey with $|b| \geq 2°$. The small dashes seen across the figure show the standard deviation of each point (plotted at both $\pm 1\sigma$), and hence provide a measure of the uniformity of the polarized intensities in each bin.

A number of interesting, large-scale features can be identified from Fig. 9. Note also that, by comparing both curves, it can be seen that the low-and high-latitude polarization values often differ markedly.

Around 265° longitude, bright, polarized emission is observed from the Vela SNR. Interestingly, if Vela were not present in this region of the plane, it appears that a nearly constant level of polarized flux would be detected between longitudes of 238° and 273°. A similar 'minimum' of approximately 40 mJy beam area^{-1} can be seen near both 295° and 345° longitude. These minima in the distribution of polarized intensities are also characterized by almost identi-
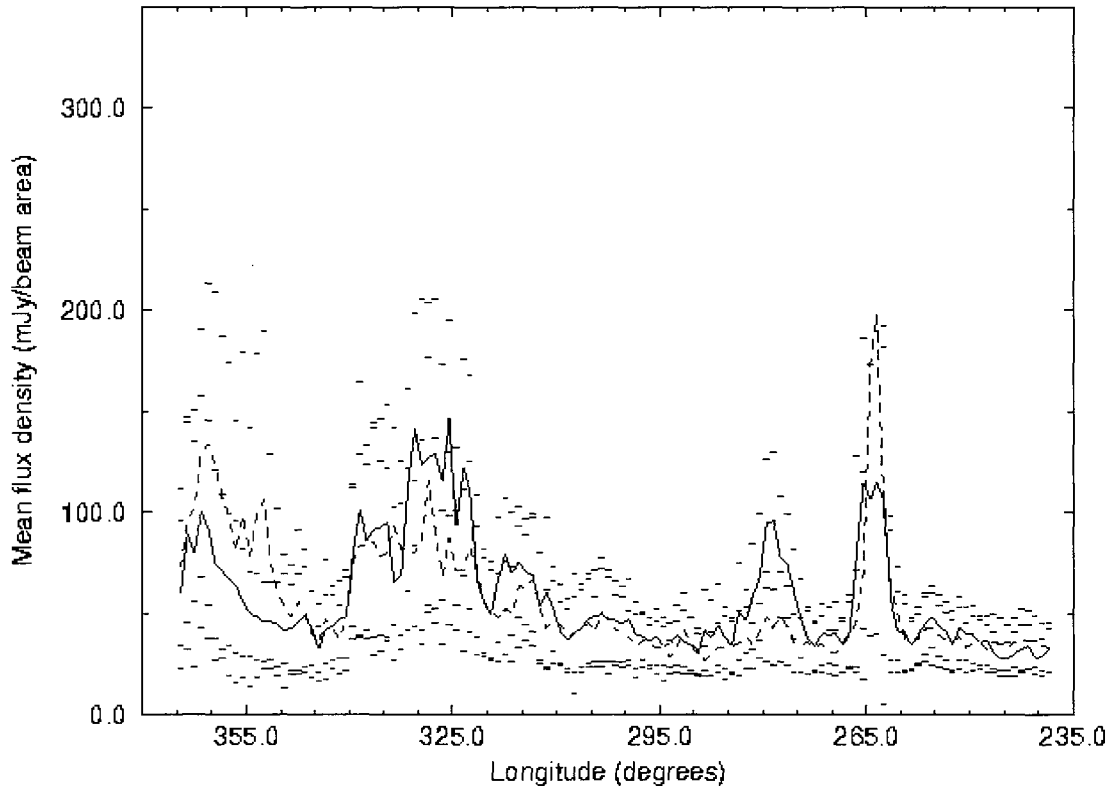
Figure 9. Mean polarized intensity values over the Galactic plane, from the 2.4-GHz survey, binned into 1° intervals of longitude (see Section 6.1.1). The dashed line shows the mean values of points with $|b| \geq 2°$; the solid line is for points with $|b| \leq 2°$. The small dashes seen across the graph indicate the standard deviation of each point (these are placed at both $\pm 1\sigma$), and hence provide a measure of the uniformity of the polarized intensities in each bin.

cal polarized fluxes in the low- and high-latitude curves. The standard deviations are also smallest in these regions, showing that the polarized intensity values are more constant over these longitudes.

These data suggest that, over much of the longitude range covered by the survey, there exists a 'background' level of polarized emission. This 'background' component is independent of latitude (over the range of latitudes examined by the survey observations), and is nearly constant over the length of the survey. The isotropic nature of this component implies a relatively local origin for the emission – certainly within several kiloparsecs. Mathewson & Milne (1965) concluded that much of the polarized emission they detected at 408 MHz was also of local origin. Hence it is possible that we are detecting smaller angular scale components of the same local emission.

Other, brighter polarization features appear superposed on this background, some of which correspond to large and bright sources of emission (again, see Fig. 9). Apart from the Vela SNR, a bright feature appears between longitudes of 275° and 282°. This is predominantly at low latitudes. Moving east of longitude 300° the polarized intensity rises, before a rapid drop back to approximately 40 mJy beam area^{-1} at $l = 340°$. Near the eastern limit of the survey, the features between 350° and 5° result from the bright 'plume' or 'cap' structure seen on the eastern side of Fig. 3.

6.1.2 Comparison with similar data from the northern plane

Interestingly, the distribution of low-latitude polarized emission ($|b| \leq 1°.4$) has been examined for part of the first Galactic quadrant by Junkes, Fürst & Reich (1987b, 1990). These authors present data showing the distribution of polarized intensities between longitudes of 10° and 75°, and it is of interest to compare this distribution with that from the 2.4-GHz Parkes survey.

The low-latitude curve in Fig. 9 shows the distribution of polarized intensities along the southern plane, over a similar latitude range to that used by Junkes et al. (1987b).

The polarized intensity values seen over the northern plane by Junkes et al. (1987b) appear similar in magnitude to those seen over the south; however, the distribution of the intensities appears quite different. The plot given by Junkes et al. (1990) shows the polarized intensity values generally decreasing towards lower longitudes (i.e. towards the Galactic Centre). This was interpreted as depolarization caused by an increasing amount of thermal material along the line of sight. Interestingly, such behaviour is not seen in the low-latitude data from the southern plane (Fig. 9); indeed, the amount of polarized emission seen in the survey generally increases towards the Galactic Centre. The abrupt drop in polarized intensities seen near 340° longitude (Fig. 9) is difficult to reconcile with depolarization, because the low- and high-latitude curves change almost identically. This would require similar depolarizations (and hence thermal electron densities) in both latitude ranges – which seems rather unlikely, unless the depolarization is very nearby.

We have interpreted our polarization data as showing a 'background' level of polarization, upon which other, brighter sources of polarized emission are superposed.

Although any further conclusions must await a more detailed analysis of the Effelsberg survey data, it is possible that the same is also true for the northern plane.

6.1.3 Distribution of vector orientations

The distribution of vector orientations along the plane, averaged into 1° intervals of Galactic longitude, is detailed in Fig. 10. As with the polarized intensity distribution, seen in Fig. 9, mean values for both low latitudes ($|b| \leq 2°$) and high latitudes ($|b| \geq 2°$) are given. The small dashes seen across the graph show the standard deviation at each point in the curve, and are plotted at both $\pm 1\sigma$.

Fig. 10 displays some interesting structure. Note that the standard deviations are quite large, indicating a wide range of vector orientations, as expected. In the presence of such large standard deviations, it is the constancy of position angles over a number of bins that is indicative of real structure; Fig. 10 shows several such regions. It is interesting to note that no area of the survey is dominated by vectors oriented at $\pm 90°$; that is, with a magnetic field perpendicular to the plane (assuming no significant Faraday rotation).

To the western side of the survey, a large negative excursion of the vector angles is visible between longitudes of 245° and 260°; this corresponds to the Gum nebula (Gum 1952). The paper by Duncan et al. (1996), in which the polarimetric emission from the Gum is discussed in detail, notes the constancy of the vector orientations over this region of the plane. Hence the appearance of this feature in Fig. 10 is not unexpected.

Between longitudes of 275° and 282°, another area of approximately constant vector orientation can be seen. This corresponds to the bright region visible in Fig. 9 between similar Galactic longitudes.

Beween 290° and 310° longitude, very unusual structure is detected in the low-latitude position angles. This takes the form of an almost symmetric transition in vector orientations, first to negative and then to positive values. Indeed, over 10° of Galactic longitude, the angles change from $-50°$ to $+40°$. The smoothness of this change from one extremum to the other, as well as the symmetry of the structure, makes this a most intriguing feature.

At around 300° longitude, corresponding to the centre of symmetry of the feature, there is nothing notable in the local Galactic magnetic field (Mathewson & Ford 1970; Sofue & Fujimoto 1983; Han & Qiao 1994). Perhaps, then, this feature is related to the magnetic field characteristics of more distant spiral arms.

It is known that at a longitude of approximately 302° we cross from the Carina spiral arm into the Centaurus arm (e.g. see fig. 4 of Paper I), the tangent points of which both lie at approximately 6 kpc. The magnetic field runs in opposite directions along these spiral arms (e.g. Han & Qiao 1994), and hence large changes in the rotation measures (RMs) may be expected as we move from one arm to the next. We suggest that the feature seen between longitudes of 290° and 310° in Fig. 10 is the result of the changing RM seen when looking almost tangentially to these spiral arms.

Now, the change in position angle from one extremum to the other is approximately 90°. At 2.4 GHz, this corresponds
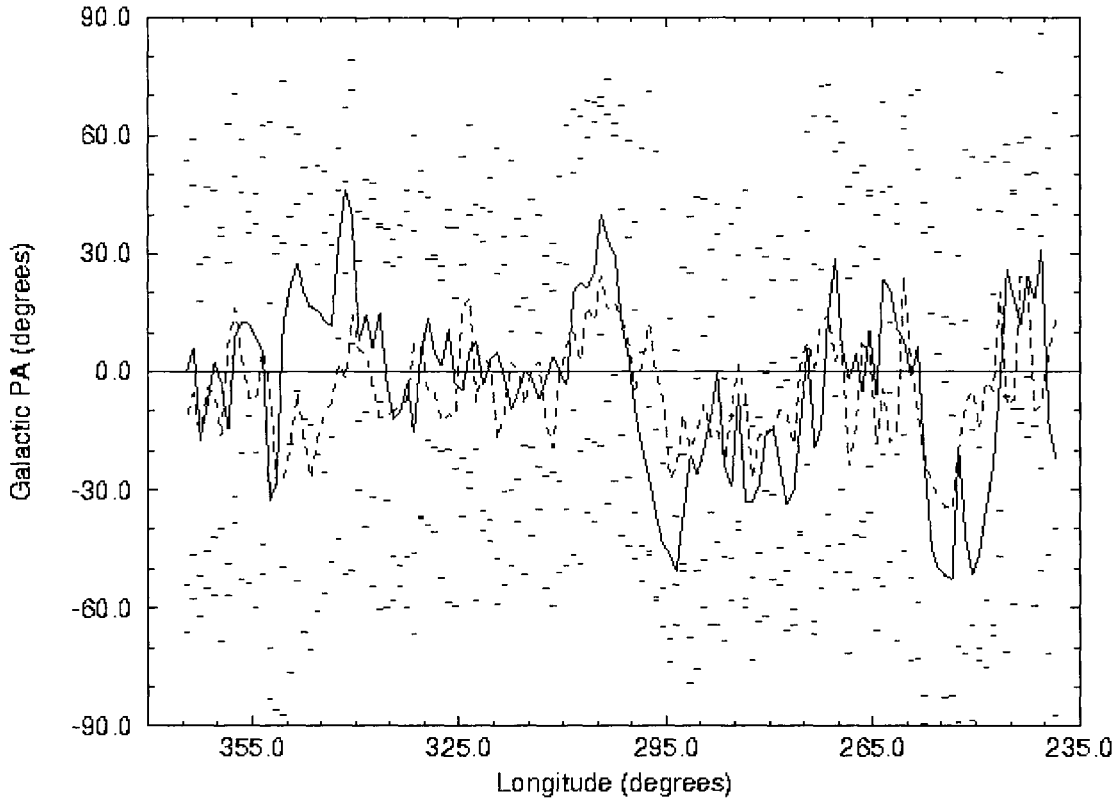
Figure 10. The distribution of polarization position angles along the Galactic plane (see Section 6.1.3). The values are from the 2.4-GHz survey, binned in 1° intervals of longitude, and show the orientation of the magnetic vector. The dashed line shows the mean values of points with $|b| \geq 2°$; the solid line is for points with $|b| \leq 2°$. A vector of angle 0° is oriented parallel to the Galactic plane, and rotates anticlockwise as the angle increases. The small dashes scattered across the graph indicate the standard deviation of each point (these are placed at both $\pm 1\sigma$).

to a change in RM across the structure of 100 rad m^{-2}. If we assume a magnetic field in both the Carina and Centaurus arms of 1.5 µG (oppositely directed: Han & Qiao 1994) and a mean interstellar thermal electron density of 0.03 cm^{-3} in each arm (e.g. Harding & Harding 1982), we calculate a maximum effective path length for the rotated emission along each arm of 1.4 kpc; this is quite a reasonable value. Furthermore, the polarity of the structure and the signs of the RMs agree with those expected for the magnetic field directions along the arms.

Further towards the eastern side, between longitudes of 340° and 350°, another region showing structure in the vector orientations can be seen. In this instance, the mean angles take on positive values. Noting that nothing similar is apparent in the high-latitude position angle plot, this feature is possibly also associated with distant Galactic structure.

As can be seen from Fig. 10, most of these regions appear more prominent (i.e. the vector orientations are more constant from one bin to the next) at low Galactic latitudes. It is interesting to note that the regions of the plane exhibiting the most striking position angle behaviour are those with the minimum polarized intensities. This point will be discussed in following sections.

The presence of coherent features within the vector angle distribution, and their identification with structures lying at

various distances, shows that this technique may hold some promise for investigations of large-scale magnetic field and RM structures in our Galaxy, over a range of distances.

6.2 Bipolar outflows from bright H ıı regions

Between Galactic longitudes of 280° and 295°, several bright H ıı complexes are visible. These H ıı complexes lie on the Carina spiral arm, at distances between 3 and 5 kpc (Caswell & Haynes 1987). The central of the three bright regions, at around 288° longitude, is the closest. The positions and kinematic distances of these H ıı complexes are given in Table 2 (distances are taken from Caswell & Haynes 1987).

Examination of the polarized intensity image of this area (Fig. 6) shows a curious pattern of regions with little polarized emission. The features can be more easily seen in Fig. 11, which shows the Stokes Q image of the area.

Several 'fan-like', bipolar extensions can clearly be seen in the image. Whilst exhibiting different collimations, the structures all appear oriented nearly perpendicular to the plane. Furthermore, these extensions appear to emanate from the bright H ıı complexes at low latitudes.

Because these 'plume' structures are detected as reductions in the level of background polarized emission at low latitudes, we conclude that these features represent out-

Table 2. The positions and distances of the three bright H II complexes thought to be causing the 'plumes' visible in Fig. 11. Distances are taken from Caswell & Haynes (1987).

Position	Distance
G284.14 − 0.63	5.1 kpc
G287.5 − 0.6	3.0 kpc
G291.28 − 0.71	3.6 kpc

flows of thermal material from the H II complexes, with emission measures sufficient to depolarize significantly the radiation passing through them at a frequency of 2.4 GHz.

The most prominent 'plumes' are associated with the H II complexes near longitudes 288° and 292°; these are the closest of the three complexes (see Table 2). The H II complex near 284° longitude lies at the greatest distance, and this exhibits a weaker and more indistinct plume.

If these thermal outflows completely depolarize the emission passing through them, then the polarized intensities just inside and just beyond the edges of each plume would allow estimates to be made of the synchrotron emission both in front of and beyond the H II complexes. Unfortunately, we cannot say whether this is the case. Nevertheless, the fact that the more prominent plumes are associated with the less distant H II regions suggests that the low-latitude polarized emission is produced over a range of distances.

This is because, if the thermal outflows depolarize all the emission passing through them, the polarized emission seen over a plume will result entirely from synchrotron emission between the H II complex and the observer. If the H II complex is nearby, little polarized emission will be produced in the intervening distance, and the plume will appear darker and more prominent. For a more distant plume, greater amounts of polarized emission are produced between the plume and the observer (assuming an approximately constant synchrotron emissivity), and hence the plume will appear as a lower contrast feature.

Furthermore, the detection of a plume associated with the H II complex at 5 kpc distance shows that a significant component of the polarized emission detected near this H II complex originates at distances greater than 5 kpc. This agrees with the work of Junkes et al. (1987b, 1990), who found a component of polarized emission from distances greater than 6 kpc in their low-latitude data from the 2.695-GHz Effelsberg survey of the northern Galactic plane (Junkes et al. 1987a; Reich et al. 1984).

It must be noted that the bright, continuum source near longitude 292° consists of two separate H II complexes: G291.284 − 0.713 and G291.614 − 0.525 (Caswell & Haynes 1987). The latter source, which lies at a distance of about 8.5 kpc, is approximately twice as bright as the former, which lies at a much closer 3.5 kpc. From the 2.4-GHz data, we cannot distinguish which of these H II regions is responsible for the plume seen near longitude 292°. However, given that
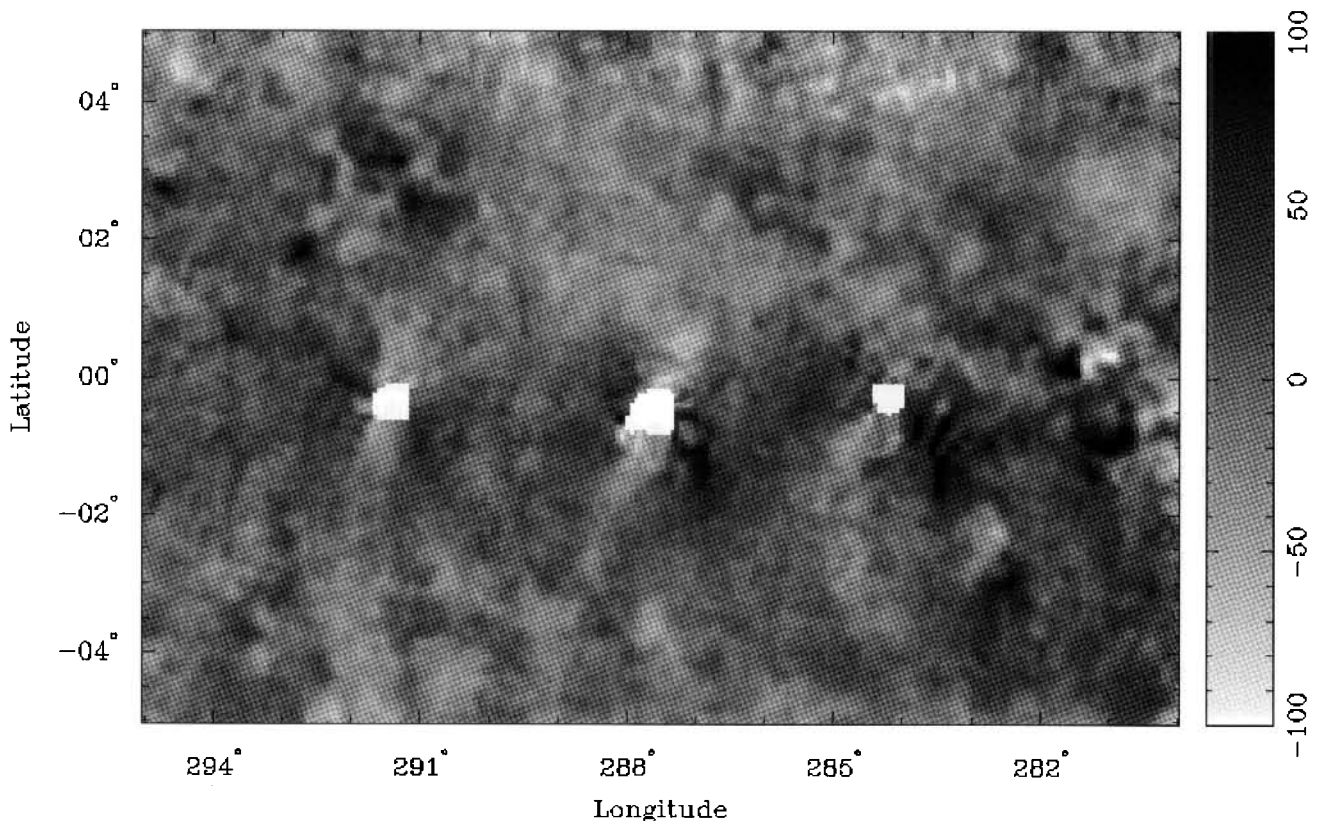
Figure 11. Stokes Q image of a region of the 2.4-GHz survey, showing three bright H II complexes (see Section 6.2). Data in the vicinity of the complexes have been blanked, and appear white. The distances to the H II regions are given in Table 2. Note the light 'channels' stretching from the H II complexes towards higher Galactic latitudes. The grey-scale wedge is labelled in units of mJy beam area^{-1}.

the other bright H II complexes (which also produce plumes) lie at distances of about 3–5 kpc, and that all three plumes appear quite similar, we consider a distance of 3.5 kpc for the plume near longitude 292° to be much more likely. Furthermore, a distance of 8.5 kpc should make the plume appear as a much less distinct feature (i.e. lower contrast), and would require a large component of the polarized emission seen in the vicinity of the plume to originate at distances beyond 8.5 kpc. Hence we identify the plume near longitude 292° with the G291.284 − 0.713 H II complex.

It is of interest to estimate the thermal electron densities within these plumes. We will confine our discussion here to the 'stem' regions of the plumes, which show the best collimation and the strongest depolarizations. First, let us assume a width for the 'stem' of a plume of the order of 1°. At the distance of these H II complexes ($\simeq 4$ kpc) this corresponds to a linear size of ≈ 70 pc.

Now, a minimum variation of $\pi/2$ rad is necessary to depolarize the emission passing through the plumes. Here it is assumed that the depolarization is caused by differential Faraday rotation on scales smaller than the telescope beam, which arises from differential thermal electron densities in and near the H II regions. Taking a longitudinal magnetic field strength of 1.5 μG (Han & Qiao 1994), we calculate a minimum thermal electron density of the order of 1 cm^{-3}. Furthermore, the density of (thermal) electrons is almost certainly less than 10 cm^{-3}, otherwise the subsquent radio emission would be visible in the total-power image of the region. Hence our 2.4-GHz data constrain the thermal electron densities within the 'stem' region of a plume to values of 1–10 cm^{-3}. Interestingly, these values agree rather well with estimates of the diffuse thermal electron density within extended H II envelopes, estimated through low-frequency recombination line work (e.g. Lockman 1976; Ananthar-amaiah 1985, 1986).

If such plume structures are indeed moving low-density, ionized material significant distances away from H II regions, these processes may help to account for the diffuse, low-density, ionized component of the interstellar medium.

6.3 The faint polarized emission

6.3.1 The nature of the faint emission

It is interesting to speculate about the origins of the faint, diffuse polarized emission detected from the 2.4-GHz survey. Even with data from a single observing frequency, it is still possible to draw a number of conclusions regarding the nature of this emission.

It was noted from Fig. 9 that the minimum polarized intensity seen over the survey (averaged into 1° intervals of longitude) was approximately 40 mJy beam area^{-1}. This minimum is evident in several sections of the survey, prompting the idea that this represents a quasi-uniform 'background' component of Galactic polarized emission, upon which the emission from other features is superposed.

This faint, polarized component generally appears as numerous regions of low surface brightness, distributed in a 'patchy' way. The vector orientations are distinctly cellular,

with cells of uniformly aligned vectors which change orientation at cell boundaries.

It is clear that the faint, low-latitude polarization contains emission from a range of distances (Section 6.2; see also Junkes et al. 1987b, 1990), out to greater than 5 kpc. Towards the higher latitudes of the survey, the faint component generally appears similar in both structure and intensity to the corresponding low-latitude emission, although presumably there is a greater proportion of nearby emission towards higher latitudes. Note that on the western side of the survey, the faint component must contain little distant emission, simply because of the smaller path length through the Galactic disc at these longitudes. However, the polarized intensities in this region of the plane may be enhanced by emission from the Gum nebula.

Qualitatively, much of the faint polarized emission visible in the 2.4-GHz images resembles that detected by Wieringa et al. (1993) using the Westerbork synthesis telescope at a frequency of 327 MHz. Specifically, a similar cellular structure in the vectors was seen, albeit on considerably different angular scales. The appearance of the features uncovered by Wieringa et al. was seen to be substantially independent of position, being observed in several separate fields at Galactic latitudes of between 16° and 35°.

It is conceivable that the faint polarization features we detect may be produced by a similar mechanism to those discussed by Wieringa et al. (1993): variations in the Faraday rotation and depolarization of the smooth synchrotron background emission, produced by a foreground 'screen'. However, this does not appear to be the case for our 2.4-GHz data. Wieringa et al. found values of RM over one region of the order of − 5 rad m^{-2}. Whilst this is sufficient to depolarize radiation significantly at 327 MHz, such a small RM produces a rotation of approximately 4° at a frequency of 2.4 GHz. Even though the RMs across the 2.4-GHz survey probably exceed a magnitude of 5 rad m^{-2}, because the survey examines regions much closer to the plane, an RM of approximately 280 rad m^{-2} would be required to produce comparable rotation at a frequency of 2.4 GHz.

Wieringa et al. favoured the 'Faraday screen' model chiefly because of the total absence of variations in the total-power emission, at least on scale-sizes comparable to those of their polarized intensity variations. This is quite definitely not the whole answer here, as can be seen in Fig. 12. This figure shows a grey-scale image of a small section of the polarized intensity survey, along with 'slices' of both the polarized intensity and total-power data. The slices were taken approximately parallel to the plane. The upper curve shows the total-power emission (in mJy beam area^{-1}), while the lower slice details the polarized intensity data (also in mJy beam area^{-1}). These slices show, for the most part, a good correlation between enhancements in the polarized intensity and total-power emission. As these slices are not atypical, we conclude that a sizeable fraction of the variations in polarized emission seen over the plane are caused by changes in the synchrotron emissivity, rather than by any depolarization or Faraday rotation of the synchrotron background. A deeper understanding of the polarized emission, and its relation to the unpolarized structure, must await a detailed correlation of the total-power and polarized intensity data, over various angular scales.
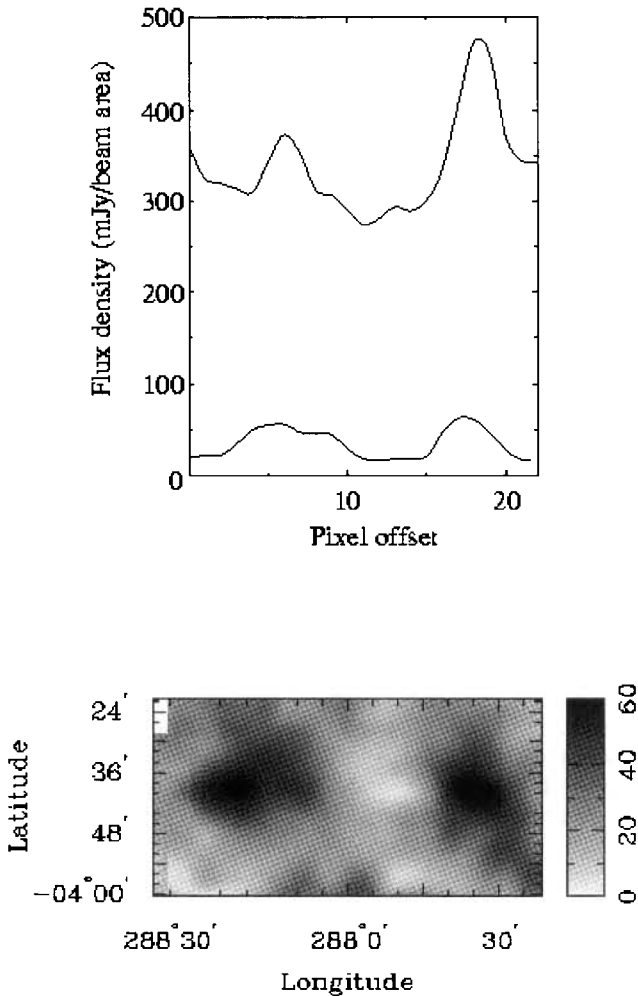
Figure 12. Grey-scale image of a small section of the polarized intensity survey images, showing a typical example of the faint 'background' emission. Above this, data from a 'slice' through the region are displayed. Slices of both total-power emission (upper curve) and polarized intensity (lower curve) are given. The slices are oriented nearly parallel to the Galactic plane. The grey-scale wedge is labelled in units of mJy beam^{-1}.

6.3.2   *Possible origins of the faint, polarized component*

There are several possibilities as to the origin of this diffuse component of polarized emission. First, the enhancements in synchrotron emission may be caused by increases in the density of relativistic electrons. Such enhancements in the source electron density could be supplied by the non-thermal electrons from the shells of ancient SNRs. In this case, the SNRs would be so highly evolved as to have completely lost their individuality, merging with the interstellar medium. Relativistic electrons are extremely long-lived particles (10^8–10^9 yr) and thus will remain in the interstellar medium long after the SNR itself has dissipated.

Alternatively, the enhancements in synchrotron emissivity may be produced by enhancements in the magnetic field strength, acting on a more uniform electron distribution (such as the electron component of cosmic rays). For synchrotron radiation with a spectral index of $\alpha = -0.7$ (typical for non-thermal electrons), the flux density varies as $B^{1.7}$;

hence modest increases in the ambient field strength (by a factor of 2, say) will produce substantial increases in the synchrotron brightness. Indeed, it is likely that both electron density and magnetic field enhancements play a role in producing the emission. This is because turbulent interstellar processes which act to increase the electron density (involving cloud interactions and collisions on many scale-sizes) will also tend to compress and twist the magnetic field. Note that we cannot comment on the relative importance of these mechanisms from the 2.4-GHz data alone.

The distribution of vector orientations along the plane, as given in Fig. 10, also provides valuable clues as to the nature of this faint polarization. Comparing Figs 9 and 10, it can be seen that the strongest patterns in the vector angles correlate with the regions of the survey in which the polarized emission is very low (near the minimum of 40 mJy beam area^{-1}). This strongly suggests that the low-intensity component of polarized emission arises from a more uniform component of the magnetic field. In the other regions of the plane the higher intensities of polarized emission, arising from other sources with independent and uncorrelated vector orientations, 'drown out' the faint component.

Fig. 10 also shows that the most structured and coherent regions of vector orientation are seen at low latitudes ($|b| \lesssim 2°$). This suggests that the structure seen in the vector angles may be attributable to more distant emission (although the Gum nebula is known to be a local feature). Considering that a proportion of the polarized emission originates from beyond 5 kpc (see Section 6.2), this is not unreasonable.

6.4   The brightly polarized regions

Apart from the Vela SNR, visible between longitudes of 260° and 270°, the discovery of the large, bright regions of polarized emission (many hundreds of mJy beam area^{-1}) came as one of the surprises of this survey.

These bright features, sometimes appearing as discrete objects, are superposed upon the faint background of polarized emission discussed in the previous section, and have no obvious total-power counterparts. In most cases, these features possess vector orientations that are uncorrelated on scale-sizes of several degrees (see Fig. 10), and hence are unlikely to yield information on the large-scale magnetic structure of the Galaxy.

At least one of these bright regions, between longitudes of 322° and 332°, appears to be associated with a nearby SNR. The clue to this association is in Fig. 4(a), in which a curved 'spur' of polarized emission can be seen near longitude 329°, extending in the range $2° \lesssim b \lesssim 5°$. This area of the plane lies within the diffuse, eastern, total-power arc of the new, large SNR candidate G325 + 0 (Duncan et al. 1997). Furthermore, the radius of curvature of the polarized 'spur' appears very similar to that of the eastern, total-power arc.

The brightly polarized emission near the Galactic Centre is an extraordinary feature. This takes the form of a large 'plume' or 'cap' towards positive Galactic latitudes, which extends from near the Galactic Centre for 15° of longitude. The vector angles over this structure vary greatly, and are possibly indicative of a highly twisted magnetic field or large RMs. Unfortunately, we cannot estimate the distance to this

structure with our current data, and so we cannot say if this is a local feature or if it is associated with the Galactic Centre. Hope of resolving this question perhaps lies with multifrequency, polarimetric data taken surrounding the Galactic Centre by R.F. Haynes et al. (private communication). A detailed analysis of these data may provide valuable information.

Around Galactic longitudes of 275° to 283°, a bright, low-latitude polarized intensity feature can be seen (Fig. 9). Both the polarized intensity and position angle are seen to vary quite smoothly across this feature. The origin of this polarized emission is unknown; perhaps it also is related to Galactic structure, lying just off the tangent point to the Carina spiral arm. Multifrequency data will doubtless be required for a better understanding of the origins of this feature.

7 CONCLUDING REMARKS

The polarimetric images of the southern plane reveal a wealth of structure, on many scale-sizes, with both a faint background component and brighter polarized features visible. Polarized emission is found to originate from a range of distances, out to greater than 5 kpc. The discovery of the bright, large-scale features (with sizes of the order of 5° or more) is especially surprising. Whilst one of these structures can be identified with the Vela SNR, the origins and nature of the other intriguing features remain a mystery. These 2.4-GHz data must be supplemented with high-sensitivity, polarimetric observations at other frequencies in order to perform detailed investigations of these new structures, their origins and nature.

WORLD WIDE WEB

Easy access to the published survey data, in FITS format images, is now available through World Wide Web servers at either the Physics Department of The University of Queensland, or the Australia Telescope National Facility. The URLs for these sites are:

http://www.atnf.csiro.au/people/duncan
http://www.physics.uq.edu.au/people/duncan

REFERENCES

Anantharamaiah K. R., 1985, JA&A, 6, 203
Anantharamaiah K. R., 1986, JA&A, 7, 131
Baars J. W. M., Genzel R., Paulini-Toth I. I. K., Witzel A., 1977, A&A, 61, 99
Berkhuijsen E. M., Brouw W. N., Muller C. A., Tinbergen J., 1965, Bull. Astron. Inst. Neth., 17, 465
Brouw W. N., Spoelstra T. A. T., 1976, A&AS, 26, 129
Caswell J. L., Haynes R. F., 1987, A&A, 171, 261
Clark D. H., Green A. J., Caswell J. L., 1975, Aust. J. Phys. Astrophys. Suppl., 37, 75
Duncan A. R., Stewart R. T., Haynes R. F., Jones K. L., 1995, MNRAS, 277, 36 (Paper I)
Duncan A. R., Stewart R. T., Haynes R. F., Jones K, L., 1996, MNRAS, 280, 252
Duncan A. R., Stewart R. T., Haynes R. F., Jones K. L., 1997, MNRAS, 287, 722
Emerson D. T., Gräve R., 1988, A&A, 190, 353
Frail D. A., Goss W. M., Whiteoak J. B. Z., 1994, ApJ, 437, 781
Gum C. S., 1952, Observatory, 72, 151
Han J. L., Qiao G. J., 1994, A&A, 288, 759
Harding D. S., Harding A. K., 1982, ApJ, 257, 603
Haslam C. G. T., 1974, A&AS, 15, 333
Haynes R. F., Stewart R. T., Gray A. D., Reich W., Reich P., Mebold U., 1992, A&A, 264, 500
Jonas J. L., de Jager G., Baart E. E., 1985, A&AS, 62, 105
Junkes N., Fürst E., Reich W., 1987a, A&AS, 69, 451
Junkes N., Fürst E., Reich W., 1987b, in Beck R., Gräve R., eds, Interstellar Magnetic Fields: Observation and Theory. Springer-Verlag, Berlin, p. 115
Junkes N., Fürst E., Reich W., 1990, in Beck R., Kronberg P. P., Wielebinski R., eds, Proc. IAU Sump. 140, Galactic and Intergalactic Magnetic Fields. Kluwer, Dordrecht, p. 63
Kühr H., Witzel A., Pauliny-Toth I. I. K., Nauber U., 1981, A&AS, 45, 367
Lockman F. J., 1976, ApJ, 209, 429
McAdam W. B., Osborne J. L., Parkinson M. L., 1993, Nat, 361, 516
Mathewson D. A., Ford V. L., 1970, Mem. R. Astron. Soc., 74, 139
Mathewson D. A., Milne D. K., 1965, Aust. J. Phys., 18, 635
Milne D. K., Caswell J. L., Kesteven M. J., Haynes R. F., Roger R. S., 1989, Proc. Astron. Soc. Aust., 8, 187
Reich W., Fürst E., Steffen P., Reif K., Haslam C. G. T., 1984, A&AS, 58, 197
Reynolds J. E., 1994, ATNF Technical Memorandum, AT/39/3/040
Sinclair M. W., Graves G. R., Gough R. G., Moorey G. G., 1992, J. Electr. Electron. Eng. Aust., 12, 147
Sofue Y., Fujimoto M., 1983, ApJ, 265, 722
Spoelstra T. A. T., 1971, A&A, 13, 373
Tabara H., Inoue M., 1980, A&AS, 39, 379
Tsuboi M., Inoue M., Handa T., Tabara H., Kato T., Sofue Y., Kaifu N., 1986, AJ, 92, 818
Westerhout G., Seeger Ch. L., Brouw W. N., Tinbergen J., 1962, Bull. Astron. Inst. Neth., 16, 187
Wielebinski R., Shakeshaft J. R., 1964, MNRAS, 128, 19
Wieringa M. H., de Bruyn A. G., Jansen D., Brouw W. N., Katgert P., 1993, A&A, 268, 215